Complex magnetic ground state of CuB_2O_4

M. Boehm*
Laboratory for Neutron Scattering, ETH Zurich & Paul Scherrer Institute, CH-5232 Villigen, Switzerland and Institut Laue-Langevin, 6 rue Jules Horowitz, BP 156, 38042 Grenoble, Cedex 9, France

B. Roessli and J. Schefer
Laboratory for Neutron Scattering, ETH Zurich & Paul Scherrer Institute, CH-5232 Villigen, Switzerland

A. S. Wills
Department of Chemistry, University College London, WC1H 0AJ London, United Kingdom

B. Ouladdiaf and E. Lelièvre-Berna
Institut Laue-Langevin, 6 rue Jules Horowitz, BP 156, 38042 Grenoble, Cedex 9, France

U. Staub
Swiss Light Source, Paul Scherrer Institute, CH-5232 Villigen, Switzerland

G. A. Petrakovskii
Institute of Physics, SB RAS, 660036 Krasnoyarsk, Russia
(Received 24 January 2003; published 3 July 2003)

The magnetic ground-state of copper metaborate CuB_2O_4 was investigated with unpolarized and polarized neutron scattering. A phase transition was found at $T_N = 21$ K to a commensurate weakly ferromagnetic state followed by a second transition at $T^* = 10$ K to an incommensurate magnetic structure. Neutron diffraction revealed a continuously changing magnetic propagation vector below T^*, and unusually asymmetric magnetic satellite reflections. Additionally, diffuse scattering is observed in the temperature range 1.5 K$\leqslant T \leqslant$30 K. The magnetic structure determined in both phases are shown to be consistent with results of symmetry analysis. In particular, we find that only one of the two inequivalent Cu^{2+} sublattice fully orders down to the lowest temperature. Our results show that the complex magnetic behavior of copper metaborate is a consequence of mutual interaction between the two Cu^{2+} sublattices with different ordering temperatures.

DOI: 10.1103/PhysRevB.68.024405 PACS number(s): 75.25.+z, 75.30.Gw, 75.10.Hk

I. INTRODUCTION

Investigation of the magnetic properties of copper metaborate, CuB_2O_4, by means of susceptibility, specific heat, and μSR spectroscopy has revealed a series of unconventional magnetic phase transitions at $T_N = 21$ K, $T^* = 10$ K, and $T \sim 1.8$ K.[1] Whereas preliminary neutron diffraction experiments showed that in the temperature regime $T^* \leqslant T \leqslant T_N$ the magnetic structure is commensurate with the nuclear lattice, it turned out that upon lowering the temperature below T^* the magnetic structure of CuB_2O_4 becomes incommensurate: the propagation vector is along the $\mathbf{c}^*$ axis and varies continuously between $\mathbf{k}_0 = (0,0,0)$ at T^* and $\mathbf{k}_0 = (0,0,0.15)$ (r.l.u.) at $T = 1.8$ K. Higher-order satellites $3\mathbf{k_0}$ were observed for temperatures close to the incommensurate-commensurate phase transition, which showed that copper metaborate forms a magnetic soliton lattice at low temperatures.[2]

It is the aim of this paper to give a detailed analysis of the magnetic structures of CuB_2O_4. We focus on the evolution of the spin arrangement in the temperature range 2 K$\leqslant T \leqslant$21 K in order to understand the complex magnetic interactions in CuB_2O_4. We note that due to the small size of the magnetic moment of Cu^{2+}, the magnetic response in diffraction experiments is weak. As the nuclear and magnetic structures both contribute to the same reflections in the case of a zero propagation vector, symmetry arguments are particularly useful. They not only separate the spin degrees of freedom into distinct symmetry-allowed models, they reduce the set of refined variables to the smallest number required to define it. The correlations between the nuclear and magnetic structures are thereby minimized. Results for the magnetic structure of copper metaborate in the commensurate phase have been briefly discussed earlier.[2,3] In this work the complete analysis of the commensurate phase is given and further extended to the incommensurate phase. We show that the symmetry arguments are consistent with the experimental results of the neutron diffraction experiments. A remaining ambiguity in the analysis of the magnetic structure in the incommensurate phase was lifted by using spherical neutron polarimetry (SNP),[4] which allows one to determine the change in orientation of the neutron polarization before and after the scattering process and, thus, to take full advantage of the information contained within Blume's equation for polarized neutron beams.[5] Finally, in the last part of this work, we will show the presence of one-dimensional diffuse scattering over an unusual large temperature range, namely from $T \sim 30$ K, i.e., well above the three-dimensional ordering temperature T_N, down to $T = 1.8$ K. This indicates that

short-range magnetic order coexists with three-dimensional long-range magnetic ordering below T_N.

II. EXPERIMENTAL DETAILS

The chemical and magnetic structures of copper metaborate were determined by neutron diffraction from both polycrystalline and single crystal samples. In order to reduce neutron absorption from natural boron, the samples were prepared with the isotope ^{11}B at the Institute of Physics in Krasnoyarsk. The powder diffraction experiments were performed on the high-resolution D1A (wavelength $\lambda = 1.91$ Å) and high-intensity (wavelength $\lambda = 2.522$ Å) D1B diffractometers at the neutron source of the Institut Laue-Langevin (ILL) using ~ 15 g of polycrystalline material. The information obtained from the powder measurements, however, turned out to be insufficient to determine the magnetic structure of CuB_2O_4. We therefore performed additional measurements on a single-crystal using the four-circle diffractometer D10 (ILL). The measurements at very low temperatures were done with the help of the 4-circle dilution cryostat of D10. For these measurements, the neutron beam was monochromatized using a graphite monochromator at the incident wavelength $\lambda = 2.36$ Å. A pyrolytic graphite filter was installed in the neutron beam to suppress contamination by higher-order wavelengths. Because the single crystal had a large volume (~ 0.5 cm^3) and an excellent mosaic, the data had to be corrected for extinction. The refinement of the chemical and magnetic structures of CuB_2O_4 were performed with the program FULLPROF (Ref. 6) and CCSL Cambridge Library.[7] Group theory calculations were performed with the help of SARAh.[8]

The SNP experiment was carried out on the polarized neutron diffractometer D3 (ILL). Neutrons are monochromatized and polarized by a $(Co_{0.92}/Fe_{0.08})$-monochromator. We note that the transverse components of the neutron polarization can only be measured if the sample is placed in a zero-field chamber (CRYOPAD), which has been developed at the ILL.[4] The polarization $\mathbf{P}_f$ of the scattered neutrons is analyzed by a ^{3}He-spin filter (Decpol). For a detailed description of CRYOPAD and Decpol we refer to Refs. 9 and 4.

Subsequent diffuse neutron measurements were performed at the neutron spallation source SINQ on the triple-axis spectrometer TASP operated in the elastic mode. The measurements were performed with the incident neutron wavenumber $k_i = 1.97$ Å^{-1}. Although contamination by higher order neutrons is low as the instrument is located on a cold source, a graphite filter of 10 cm length was installed both in the incoming beam to eliminate residual high-energy neutrons. A collimation of 80' was installed in the incident and scattered beam. The same single crystal was used as before. It was oriented with the crystallographic axis [110] perpendicular to the scattering plane.

III. CHEMICAL STRUCTURE

A neutron powder diffraction pattern taken at $T = 45$ K on the high-resolution powder diffractomer D1A is shown in Fig. 1. The chemical structure can be described within the tetragonal space-group $I\bar{4}2d$, in agreement with previous

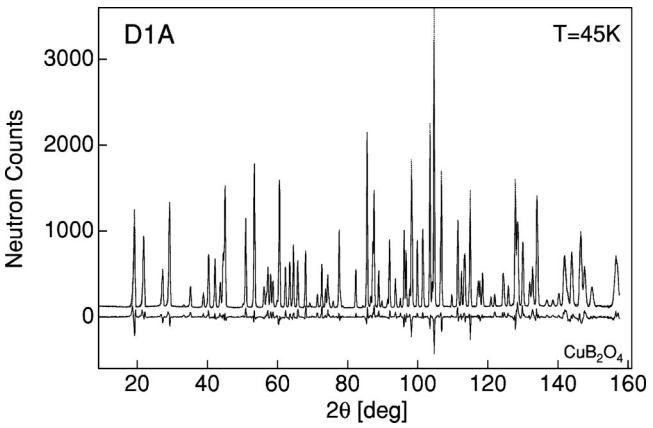

FIG. 1. Neutron powder diffraction pattern taken at $T = 45$ K in CuB_2O_4 shown together with a refinement of the data.

x-ray data[10] taken at room temperature. From the point of view of the magnetic properties, it is essential to recognize that CuB_2O_4 crystallizes with copper ions situated at two inequivalent crystallographic positions (see Fig. 2), hereafter denoted Cu(A) and Cu(B), respectively. The Cu(A) ions are located at site $4b$ (point symmetry S_4;$00\frac{1}{2}$), Cu(B)'s at site $8d$ (point symmetry C_2;$x\frac{1}{4}\frac{1}{8}$, $x = 0.0815$) (see Table I). The Cu(A) ions are at the center of square units formed by four oxygens with a 90° O-Cu(A)-O angle and a Cu(A)-O distance of 1.942 Å. Cu(B) has a similar environment, but in this case the oxygen ions form a slightly distorted square unit, which is almost confined within the [100] or [010] planes. We note that down to $T = 1.5$ K no distortion of the tetragonal structure has been observed.

IV. MAGNETIC GROUND-STATE IN ZERO-FIELD

A. Magnetic structure in the commensurate phase

Figure 3 shows neutron powder diffraction patterns taken at $T = 35$ and 12 K, respectively, i.e., above and below the

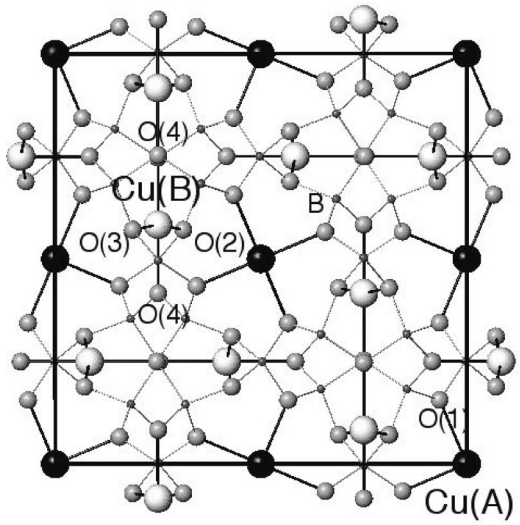

FIG. 2. Projection of the chemical structure of CuB_2O_4 at onto the basal plane of the tetragonal unit cell.

TABLE I. Atomic positions x,z, and y in the unit cell of CuB_2O_4 (space group: $I\bar{4}2d$). B: isotropic Debye-Waller factor.

Atom	x	y	z	B	Occupancy
Cu(A)	0.000	0.000	0.500	0.37	0.25
Cu(B)	0.083(1)	0.250	0.125	0.85	0.50
O(1)	0.156(2)	0.066(1)	0.498(3)	0.36	1.00
O(2)	0.253(2)	0.250	0.625	0.56	0.50
O(3)	0.250	0.084(2)	0.875	0.23	0.50
O(4)	0.071(1)	0.189(1)	0.789(3)	0.48	1.00
B(1)	0.183(1)	0.146(1)	0.702(2)	0.07	1.00
B(2)	−0.003(3)	0.250	0.625	0.80	0.50

Néel temperature $T_N \sim 21$ K. Below the Néel temperature an additional reflection is indexed as (1,1,0) in the chemical cell. This Bragg peak is forbidden in the $I\bar{4}2d$ space group due to special extinction rules. As this restriction also holds for a ferromagnetic arrangement, the reflection indicates an antiferromagnetic ordering in CuB_2O_4. Further very weak reflections could be indexed using the Miller indices of the chemical lattice which indicates that the magnetic and chemical cell coincide. The propagation vector of the magnetic structure is therefore $\mathbf{k}_0=(0,0,0)$. The space group $I\bar{4}2d$ contains eight symmetry elements and has five irreducible representations. Four of these are one-dimensional (Γ_1 $-\Gamma_4$) and one (Γ_5) is two dimensional (see Table II). In the symmetry analysis the magnetic moment within the magnetic unit cell is considered as an axial vector. Every component of the n axial vectors in the unit cell transforms into each other by the symmetry elements of the group. These transformations can be represented by $3n$ dimensional matrices, termed the 'magnetic representation', which is in general reducible. Using group theory, the magnetic representation can be decomposed into the irreducible representations of the paramagnetic group. The basis vectors which span the space of a given irreducible representation are obtained by the projection operator technique (see, e.g., Ref. 11). For CuB_2O_4 this decomposition, when applied for the Cu(A) moments, gives

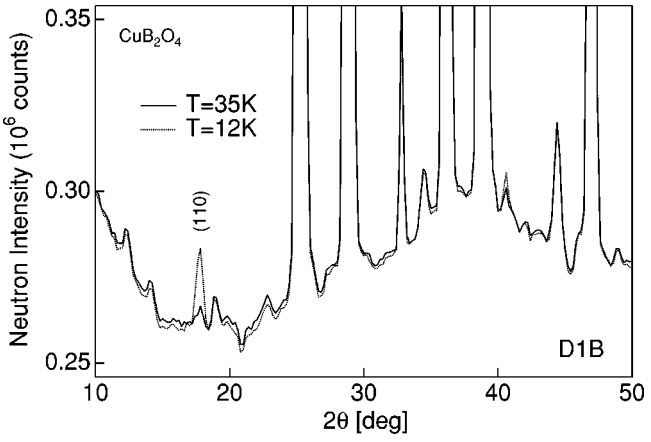

FIG. 3. Comparison of neutron powder diffraction patterns measured in CuB_2O_4 at $T=35$ and 12 K, respectively. Note the additional peak at $2\theta=17°$ for $T=12$ K.

TABLE II. Character table of space group D_{2d}^{12} (taken from Ref. 12).

D_{2d}^{12}	E	C_{2z}	S_{4z}^{-}	S_{4z}^{+}	C_{2y}	C_{2x}	σ_{da}	σ_{db}
Γ_1	1	1	1	1	1	1	1	1
Γ_2	1	1	1	1	−1	−1	−1	−1
Γ_3	1	1	−1	−1	1	1	−1	−1
Γ_4	1	1	−1	−1	−1	−1	1	1
Γ_5	2	−2	0	0	0	0	0	0

$$\Gamma_A=\Gamma_1+\Gamma_2+2\Gamma_5, \tag{1}$$

and, for Cu(B),

$$\Gamma_B=\Gamma_1+2\Gamma_2+2\Gamma_3+\Gamma_4+3\Gamma_5, \tag{2}$$

respectively. The corresponding basis vectors are given in Tables III and IV. As the linear combinations of the basis vectors are the Fourier components of the magnetic moments, they can be transformed into real magnetic moments by the summation

$$\mathbf{m_l}=\sum_{\mathbf{k}} \mathbf{m^k}\exp\{-i\mathbf{k}\cdot\mathbf{l}\}, \tag{3}$$

with $\mathbf{l}=n_1\mathbf{a}+n_2\mathbf{b}+n_3\mathbf{c}$. The possible magnetic structures in accordance with symmetry are obtained from the basis vectors of the different representations given in Tables III and IV. The two one-dimensional basis vectors Γ_1 and Γ_2 of the Cu(A) site correspond to an antiferromagnetic and a ferromagnetic arrangement of the spins along the tetragonal **c** axis, respectively. The two-dimensional representation Γ_5 has two basis vectors. Whereas the first one, $\psi_{AI}(\Gamma_5)$, describes a ferromagnetic alignment of the magnetic moments in the tetragonal basal plane, the second vector $\psi_{AII}(\Gamma_5)$, which is orthogonal to the first one, corresponds to an antiferromagnetic magnetic structure. It is a property of symmetry that any linear combination of basis vectors,

$$\psi=\sum_i c_i\psi_i, \tag{4}$$

associated with an irreducible representation also follows the symmetry of that irreducible representation. Hence, depending on the values of the coefficients c_i, every canted spin

TABLE III. Basis vectors of CuB_2O_4 at lattice site A in the commensurate phase ($\mathbf{k}=0$). $\boldsymbol{\psi}_{AI}(\Gamma_5)=[\psi_1(\Gamma_5),\psi_2(\Gamma_5)]$; $\boldsymbol{\psi}_{AII}(\Gamma_5)=[\psi_3(\Gamma_5),\psi_4(\Gamma_5)]$.

Γ_1:	$\psi_1(\Gamma_1)$	$S_{A1z}-S_{A2z}$,
Γ_2:	$\psi_1(\Gamma_2)$	$S_{A1z}+S_{A2z}$,
Γ_5:	$\psi_1(\Gamma_5)$	$S_{A1x}+S_{A2x}$,
	$\psi_2(\Gamma_5)$	$-S_{A1y}-S_{A2y}$,
	$\psi_3(\Gamma_5)$	$S_{A1y}-S_{A2y}$,
	$\psi_4(\Gamma_5)$	$S_{A1x}-S_{A2x}$.

TABLE IV. Basis vectors of CuB_2O_4 at lattice site B in the commensurate phase ($\mathbf{k}=0$). $\boldsymbol{\psi}_{BI}(\Gamma_5)=[\psi_1(\Gamma_5),\psi_2(\Gamma_5)]$; $\boldsymbol{\psi}_{BII}(\Gamma_5)=[\psi_3(\Gamma_5),\psi_4(\Gamma_5)]$; $\boldsymbol{\psi}_{BIII}(\Gamma_5)=[\psi_5(\Gamma_5),\psi_6(\Gamma_5)]$.

Γ_1:	$\psi_1(\Gamma_1)$	$S_{B1x}-S_{B2x}+S_{B3y}-S_{B4y}$,
Γ_2:	$\psi_1(\Gamma_2)$	$S_{B1y}-S_{B2y}-S_{B3x}+S_{B4x}$,
	$\psi_2(\Gamma_2)$	$S_{B1z}+S_{B2z}+S_{B3z}+S_{B4z}$,
Γ_3:	$\psi_1(\Gamma_3)$	$S_{B1y}-S_{B2y}+S_{B3x}-S_{B4x}$,
	$\psi_2(\Gamma_3)$	$S_{B1z}+S_{B2z}-S_{B3z}-S_{B4z}$,
Γ_4:	$\psi_1(\Gamma_4)$	$S_{B1x}-S_{B2x}-S_{B3y}+S_{B4y}$,
Γ_5:	$\psi_1(\Gamma_5)$	$S_{B1x}+S_{B2x}$,
	$\psi_2(\Gamma_5)$	$-S_{B3y}-S_{B4y}$,
	$\psi_3(\Gamma_5)$	$S_{B3x}+S_{B4x}$,
	$\psi_4(\Gamma_5)$	$-S_{B1y}-S_{B2y}$,
	$\psi_5(\Gamma_5)$	$S_{B3z}-S_{B4z}$,
	$\psi_6(\Gamma_5)$	$S_{B1z}-S_{B2z}$.

alignment, ranging from an antiferromagnet over a 90° canted structure to a ferromagnet, in the basal plane is described by Γ_5.

As single crystal magnetization measurements show a weak ferromagnetic moment of ~0.56 emu/g (at $T=12$ K) in the basal plane, the only compatible magnetic structure is a linear combination of wave functions as given in Eq. (4). The refinement of the magnetic structure using 25 magnetic Bragg reflections gave the best agreement between calculated and experimental intensities ($R_{Bragg}=5.3$, $\chi^2=1.3$) with an almost antiferromagnetic alignment of Cu(A) atoms with a small canting angle α between neighboring spins (see Table V, Fig. 4). From the quality of our data, however, any angle between $0<\alpha<10°$ yields a similar goodness of fit. The goodness-of-fit parameter worsens for more pronounced canting angles and reaches a value of $\chi^2=3.4$ for a 90° canted structure,[3] which was proposed earlier for the magnetic ground state in the commensurate phase.[2] Though the two models yield a similar quality of fits, it appears that a canting angle of $\alpha\sim3°$ corresponds to the value obtained by the magnetization measurements.[3] Additionally spin-wave calculations starting from this ground state give an excellent agreement with the experiment.[12] We note that admitting small components of Cu(A) spins along the **c** axis slightly improved the goodness-of-fit values, which suggests that the magnetic moments are not exactly confined to the tetragonal plane. Whereas at $T=12$ K, the magnetic moment for Cu(A) amounts to $\mu_{Cu(A)}=(0.86\pm0.01)\mu_B$, we find that the Cu(B)

TABLE V. Spin components of CuB_2O_4 at $T=12$ K as obtained from a least-square fit ($\chi^2=1.5$) in μ_B.

	μ_x	μ_y	μ_z	$\lvert\mu\rvert$
$Cu(A_1)$	0.601(4)	0.601(4)	0.15(2)	0.863(5)
$Cu(A_2)$	−0.601(4)	−0.601(4)	−0.15(2)	0.863(5)
$Cu(B_1)$	−0.023(3)	−0.024(3)	0.20(1)	0.20(1)
$Cu(B_2)$	−0.023(3)	−0.024(3)	−0.20(1)	0.20(1)
$Cu(B_3)$	0.023(3)	0.024(3)	0.20(1)	0.20(1)
$Cu(B_4)$	0.023(3)	0.024(3)	−0.20(1)	0.20(1)

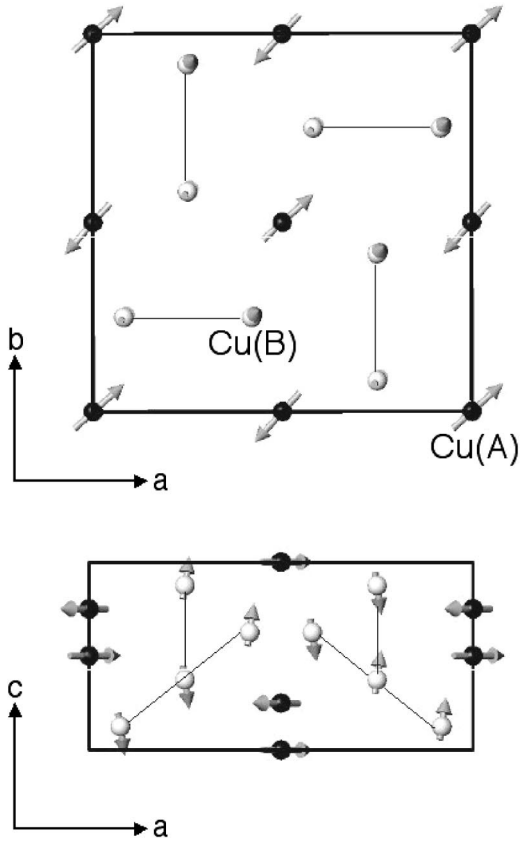

FIG. 4. Antiferromagnetic structure of CuB_2O_4 in the commensurate phase. Cu(A) and Cu(B) positions are represented by black and open symbols, respectively. The arrows mirror the directions of the magnetic moments $\boldsymbol{\mu}$.

atoms only have a small magnetic moment, $\mu_{Cu(B)}=(0.20\pm0.01)\mu_B$. This shows that the moments in the Cu(B)-sublattice are not saturated in the commensurate phase. Due to this reduced value, the influence of the Cu(B) moments on the refinements is weak and, consequently, the determination of its magnetic ordering difficult. However, we note that the Γ_5 representation for site B has three basis vectors. Two of those describe a structure where the spins are confined in the basal plane and one is along the tetragonal axis. Our refinements showed that the latter is dominating which gives an antiferromagnetic arrangement of Cu(B) moments along the **c** axis (see Fig. 4). For completeness we give a comparison between observed and calculated magnetic intensities in Table VI.

B. Magnetic structure in the incommensurate phase

Upon cooling the sample below $T^*=10$ K, we find that the magnetic reflections split into a set of two satellites, as shown in Fig. 5, indicating that the magnetic structure becomes incommensurate along the tetragonal axis of the chemical structure. The temperature dependence of the magnetic propagation vector follows an approximate power law $|\mathbf{k}_0(T)|\sim|T^*-T|^{0.5}$ down to $T\sim1.5$ K. Below this temperature the propagation vector is temperature independent with indices $\mathbf{k}_0=(0,0,0.15)$ (r.l.u.) down to the lowest measured temperature $T=200$ mK.

TABLE VI. Calculated, I_{calc}, and observed, I_{obs}, intensities in the commensurate phase. h,k, and l are the Miller indices, Δ/σ gives the difference $\Delta = I_{calc} - I_{obs}$ divided by the experimental error ($R_{Bragg} = 5.3$).

h	k	l	I_{obs}	I_{calc}	Δ/σ	h	k	l	I_{obs}	I_{calc}	Δ/σ
0	−2	−2		592		0	0	2		717	
−2	0	−2		592		0	0	2		717	
			876	1184	−1.8				1371	1434	−1.6
0	2	−2		733		0	3	0		0	
2	0	−2		733		3	0	0		0	
			1382	1466	−0.5				4	0	1
2	−2	−2		588		0	4	1		0	
−2	−2	−2		144		4	0	1		0	
			739	732	0.2				7	0	0.5
−2	−2	2		280		−1	5	1		0	
−2	2	2		588		5	1	1		0	
			815	867	−1.4				0	0	0
−2	2	2		588		−1	1	1		0	
2	2	2		144		1	1	1		0	
			681	732	−1.6				0	0	0
1	−2	−1		441		−3	3	3		0	
−2	−1	−1		204		3	3	3		0	
			568	645	−0.7				4	0	0.3
3	3	0		21		3	1	0		238	
3	−3	0		826		1	−3	0		723	
			838	847	−0.3				1024	961	2.3

1. Unpolarized neutron diffraction

To proceed with the symmetry analysis of the magnetic structure of CuB_2O_4 in the incommensurate phase, it is at first necessary to determine the set of irreducible representations of the little group, $G_{\mathbf{k}_0}$—the subgroup of the original space-group made up of the elements which leave the magnetic propagation vector $\mathbf{k}_0$ invariant. For the propagation

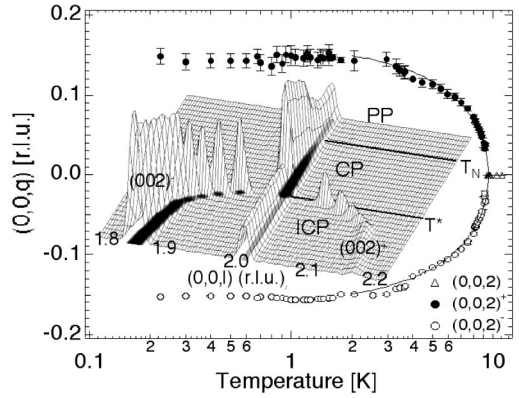

FIG. 5. Temperature dependence of the magnetic propagation vector $\mathbf{k}_0$ around the magnetic zone center (002). The inset shows the neutron intensity along the reciprocal **c** axis for different temperatures. Magnetic intensity appears at $T = 21$ K, superimposed on a small nuclear contribution. At $T = 10$ K, the magnetic reflection splits into two magnetic satellites. PP: paramagnetic phase; CP: commensurate phase; ICP: incommensurate phase.

TABLE VII. Irreducible representations of the little group $G_{\mathbf{k}}$. The phase factor ε is given by: $\varepsilon = \exp[-2\pi i \mathbf{k}_{mag} \cdot \mathbf{t}(\sigma_{da})] = \exp(-\pi i \frac{3}{2} k_z)$. $\mathbf{k}_{mag} = (0,0,k_z)$ is the magnetic propagation vector in the incommensurate phase and $\mathbf{t}(\sigma_{da}) = \mathbf{t}(\sigma_{db}) = (\frac{1}{2},0,\frac{3}{4})$ the translational component of the symmetry elements σ_{da} and σ_{db}.

	E	C_{2z}	σ_{da}	σ_{db}
Γ_1	1	1	ε	ε
Γ_2	1	1	$-\varepsilon$	$-\varepsilon$
Γ_3	1	−1	ε	$-\varepsilon$
Γ_4	1	−1	$-\varepsilon$	ε

vector $\mathbf{k}_0 = (0,0,2\pi\mu/c)$, $(\mu \in \Re \neq 0, \pm 1, \pm 2, \ldots)$, the little group $G_{\mathbf{k}_0}$ of CuB_2O_4 in the incommensurate phase contains four symmetry elements: $E, C_2, \sigma_d^2, \sigma_d^1$. The remaining symmetry operators reverse the direction of $\mathbf{k}_0$. The rotational parts of these four symmetry elements correspond to point-group $mm2$ (C_{2v} in Schoenflies notation). Using the tables of the irreducible representations of the space group given by Kovalev,[13] we find the irreducible representations of the projective (or ''loaded'') representations of $G_{\mathbf{k}_0}$, which have to be multiplied by the appropriate phase factors

$$\varphi_i = \exp(-2\pi \mathbf{k}_0 \cdot \boldsymbol{\tau}_i), \tag{5}$$

where $\boldsymbol{\tau}_i$ are the translation parts of the symmetry elements. The ''phased'' representations are given in Table VII. There are four one-dimensional representations, which can be used to construct the possible magnetic structures, in a similar way to what was done in the commensurate phase. The decomposition of these representations is

$$\Gamma_A = \Gamma_1 + \Gamma_2 + 2\Gamma_3 + 2\Gamma_4 \tag{6}$$

for the Cu(A) site and

$$\Gamma_B = 3\Gamma_1 + 3\Gamma_2 + 3\Gamma_3 + 3\Gamma_4 \tag{7}$$

for the moments on site B, respectively. The corresponding basis vectors are tabulated in Table VIII and Table IX for the Cu^{2+} ions located on sites A and B, respectively.

The possible spin arrangements for the Cu(A) moments are obtained by noting that the first two representations given in Table VIII describe longitudinal spin-density waves propagating along the tetragonal axis [see Fig. 6(a)], with the two symmetry related Cu(A) spins being either antiferromag-

TABLE VIII. Basis vectors of CuB_2O_4 at lattice site A in the incommensurate phase: $\mathbf{k}_{mag} = [0,0,k_z(T)]$. The phase $\varepsilon\varphi_1$ has the value $\varepsilon\varphi_1 = \exp(-i\frac{3}{2}\pi k_z)\exp(i2\pi k_z) = \exp(i\frac{1}{2}\pi k_z)$.

Γ_1:	$\psi_1(\Gamma_1)$	$S_{A1z} - \varepsilon\varphi_1 S_{A2z}$,
Γ_2:	$\psi(\Gamma_2)$	$S_{A1z} + \varepsilon\varphi_1 S_{A2z}$,
Γ_3:	$\psi_1(\Gamma_3)$	$S_{A1x} - \varepsilon\varphi_1 S_{A2y}$,
	$\psi_2(\Gamma_3)$	$S_{A1y} - \varepsilon\varphi_1 S_{A2x}$,
Γ_4:	$\psi_1(\Gamma_4)$	$S_{A1x} + \varepsilon\varphi_1 S_{A2y}$,
	$\psi_2(\Gamma_4)$	$S_{A1y} + \varepsilon\varphi_1 S_{A2x}$.

TABLE IX. Basis vectors of CuB_2O_4 at lattice site B in the incommensurate phase: $\mathbf{k}_{mag}=[0,0,k_z(T)]$.

Γ_1:	$\psi_1(\Gamma_1)$	$S_{B1x}-S_{B2x}+\varepsilon S_{B3y}-\varepsilon S_{B4y}$,
	$\psi_2(\Gamma_1)$	$S_{B1y}-S_{B2y}+\varepsilon S_{B3x}-\varepsilon S_{B4x}$,
	$\psi_3(\Gamma_1)$	$S_{B1z}+S_{B2z}-\varepsilon S_{B3z}-\varepsilon S_{B4z}$.
Γ_2:	$\psi_1(\Gamma_2)$	$S_{B1x}-S_{B2x}-\varepsilon S_{B3y}+\varepsilon S_{B4y}$,
	$\psi_2(\Gamma_2)$	$S_{B1y}-S_{B2y}-\varepsilon S_{B3x}+\varepsilon S_{B4x}$,
	$\psi_3(\Gamma_2)$	$S_{B1z}+S_{B2z}+\varepsilon S_{B3z}+\varepsilon S_{B4z}$.
Γ_3:	$\psi_1(\Gamma_3)$	$S_{B1x}+S_{B2x}-\varepsilon S_{B3y}-\varepsilon S_{B4y}$,
	$\psi_2(\Gamma_3)$	$S_{B1y}+S_{B2y}-\varepsilon S_{B3x}-\varepsilon S_{B4x}$,
	$\psi_3(\Gamma_3)$	$S_{B1z}-S_{B2z}+\varepsilon S_{B3z}-\varepsilon S_{B4z}$.
Γ_4:	$\psi_1(\Gamma_4)$	$S_{B1x}+S_{B2x}+\varepsilon S_{B3y}+\varepsilon S_{B4y}$,
	$\psi_2(\Gamma_4)$	$S_{B1y}+S_{B2y}+\varepsilon S_{B3x}+\varepsilon S_{B4x}$,
	$\psi_3(\Gamma_4)$	$S_{B1z}-S_{B2z}-\varepsilon S_{B3z}+\varepsilon S_{B4z}$.

netically [$\Gamma_A(1)$ representation] or ferromagnetically [$\Gamma_A(2)$ representation] orientated. Using Eqs. (3) and (4) it can be shown that the $\Gamma_A(3)$ and $\Gamma_A(4)$ representations describe a transverse spin density wave (TSW) along the **c** axis, when $c_1, c_2 \in \Re$ [Fig. 6(b)]. A simple helical structure (SH) is realized, if $|c_1|=|c_2|$ and one of the coefficient is complex, while $|c_1|\neq|c_2|$ leads to an elliptical magnetic structure. For the Cu spins on sublattice B, the variety of possible spin structures is even larger, as a third component c_3 in Eq. (4) has to be considered. For $c_3 \neq 0$, the rotation plane of the magnetic moments is no longer orthogonal to the tetragonal axis [see Fig. 6(d), $\widetilde{SH}$].

At this point of the discussion, we find it useful to write the Fourier components of the $\Gamma_A(3)$ representation in the vector form

$$\mathbf{m}_{A1}^{\mathbf{k}}=\begin{pmatrix} c_1 S_{A1x} \\ c_2 S_{A1y} \end{pmatrix}, \quad \mathbf{m}_{A2}^{\mathbf{k}}=-\begin{pmatrix} c_1 S_{A2x} \\ c_2 S_{A2y} \end{pmatrix}\cdot \exp\{i(\pi/2)k_z\}.$$

Here, S_{A1x} is the Fourier transform of the x component of the spin at the position $A1$. For $\mathbf{k}\rightarrow 0$ we note that these two vectors become identical to the basis vectors of the magnetic structure in the commensurate phase and that the phase transition at T^* is continuous. On the other hand, making the assumption that $\Gamma_A(4)$ becomes critical at T^* leads to a π phase change in $\mathbf{m}^{\mathbf{k}}_{A2}$ when $\mathbf{k}\rightarrow 0$. This situation is unlikely as the neutron intensities measured for different Bragg reflections through the commensurate-incommensurate phase transition do not exhibit any abrupt change. Because the LSW can be ruled out for the same reason, it appears that the magnetic structure of copper metaborate in the incommensurate phase is described by the $\Gamma_A(3)$ irreducible representation. Moreover, the relative phases between the magnetic moments of ions located on the same sublattice are fixed by symmetry. We are therefore left with four independent parameters to refine: the size of the magnetic moments on both sublattices, a possible component of the spins along the tetragonal axis for the Cu(B) ions, c_3, and the phase φ between $\boldsymbol{\mu}_{Cu(A)}$ and $\boldsymbol{\mu}_{Cu(B)}$. From the refinement of magnetic satellite intensities measured around 50 nuclear Bragg reflections at $T=2$ K, we find that the magnetic structure can be described by helices propagating along the tetragonal axis for both Cu(A)- and Cu(B) sublattice. The magnetic Cu(A) moments keep their orientation within the tetragonal plane and have the value $\mu_{Cu(A)}=(0.94\pm 0.06)\mu_B$. The size of the magnetic moment on the Cu(B) site is found to have increased compared to the commensurate phase. The best least-squares refinement ($R_{Bragg}=16.6$ for $T=2$ K) was obtained for a value $\mu_{Cu(B)}=(0.54\pm 0.05)\mu_B$ with $c_3=(0.27\pm 0.02)\mu_B$. Restricting the Cu(B) moments also within the tetragonal plane $c_3=0$ [$\mu_{Cu(B)}=(0.48\pm 0.05)\mu_B$] slightly decreased the goodness-of-fit value to $R_{Bragg}=16.0$, which shows that the refinement is not very sensitive to modifications on the c_3 component. The phase between the magnetic moments on the A and B sublattices for both cases has the value $\varphi=(252\pm 7)°$. The comparison between calculated and observed intensities for $c_3=0$ is shown in Table X.

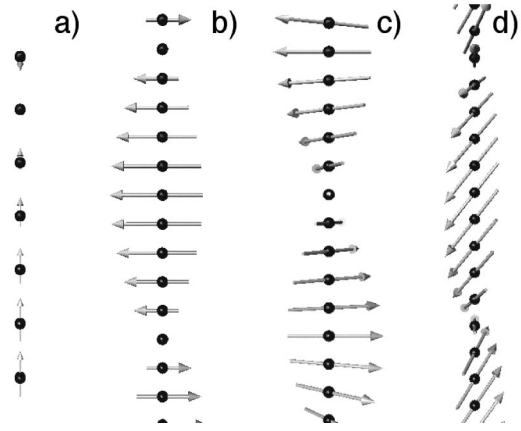

FIG. 6. Possible modulated structures along the tetragonal **c** axis, according to symmetry analysis: (a) longitudinal spin-density wave LSW, (b) transverse spin-density wave TSW, (c) simple helix SH, (d) $\widetilde{SH}$.

2. Spherical neutron polarimetry

It is important to note that it was impossible to distinguish, with standard neutron diffraction technique, between simple helices and transversal spin density waves. This is due to the fact that TSWs in a tetragonal system can have two different domains with spin alignments perpendicular to each other. When the contribution of each domain is added the magnetic structure factors become equal to those of a helical structure. To lift this ambiguity we used SNP, which allows to measure both the transverse and longitudinal components of the scattered neutron polarization beam. For pure magnetic reflections, the polarization of the scattered beam $\mathbf{P}_f$ is related to the polarization of the incident neutron beam $\mathbf{P}_i$ according to[5]

$$\mathbf{P}_f\left(\frac{d\sigma}{d\Omega}\right)=-\mathbf{P}_i(\mathbf{F}_{M\perp}\cdot\mathbf{F}^*_{M\perp})+2\Re[\mathbf{F}_{M\perp}(\mathbf{P}_i\cdot\mathbf{F}^*_{M\perp})] - i(\mathbf{F}^*_{M\perp}\times\mathbf{F}_{M\perp}), \quad (8)$$

where

TABLE X. Calculated, I_{calc}, and observed, I_{obs}, intensities from the refinement of the diffraction data in the incommensurate phase ($T=2$K). Δ/σ gives the difference $\Delta=I_{obs}-I_{calc}$ divided by the experimental error ($R_{Bragg}=12.5$).

			$\tau-\mathbf{k}_{mag}$			$\tau+\mathbf{k}_{mag}$		
h	k	l	I_{obs}	I_{calc}	Δ/σ	I_{obs}	I_{calc}	Δ/σ
−4	0	2	1693	1570	3.1			
−4	1	1	293	213	5.5	1447	1596	−3.7
−3	0	1	493	803	−10.9	709	584	5.2
−2	1	1	1972	2005	−0.7	363	493	−5.9
−2	2	2	2644	2744	−1.9			
−1	0	1	2602	2499	2.1			
0	−3	1	403	514	−4.9			
0	−2	2	1040	980	1.9	2798	2202	12.7
0	−1	1	380	118	24.2	2717	3312	−10.3
0	0	2	6900	7611	−8.2	5	34	−4.9
0	1	1				2755	3301	−9.5
0	2	2				2911	2214	14.8
1	−4	1				1272	1290	−0.5
1	−3	2				665	569	4.0
1	−2	1	2230	2645	−8.1	391	331	3.3
1	−1	2	180	19	37.0	271	23	52.4
1	0	1	383	339	2.4	2838	2498	6.8
1	1	2	114	25	17.6	156	17	33.9
2	−3	1	638	692	−2.1	675	920	−8.1
2	−2	2	479	362	6.1	2674	2757	−1.6
2	−1	1	2101	1997	2.3	425	491	−3.0
2	0	0	923	929	−0.2	831	924	−3.2
2	0	2	1011	982	0.9	2759	2210	11.7
2	1	1	2171	2116	1.2	367	550	−7.8
2	2	2	453	358	5.0	2657	2745	−1.7
3	−4	1	567	614	−1.9			
3	−2	1	682	937	−8.3	660	641	0.7
3	−1	2				651	575	3.2
3	0	1	431	803	−13.1	680	584	4.0
3	1	2	390	625	−9.4	652	569	3.5
4	−3	1	598	458	6.6			
4	−1	1	296	213	5.6	1329	1600	−6.8
4	0	0	611	321	16.2	598	321	15.5
4	0	2	1730	1570	4.0			
4	1	1	246	236	0.7	1410	1679	−6.6
5	0	1				211	46	24
5	1	0	865	915	−1.7	904	918	−0.5

$$\left(\frac{d\sigma}{d\Omega}\right)=\mathbf{F}_{M\perp}\cdot\mathbf{F}^{*}_{M\perp}+i\mathbf{P}_i(\mathbf{F}^{*}_{M\perp}\times\mathbf{F}_{M\perp}) \tag{9}$$

is the magnetic neutron cross-section. $\mathbf{F}_{M\perp}$ is the component of the magnetic structure factor orthogonal to the scattering vector $\mathbf{Q}$ and $\mathbf{F}^{*}_{M\perp}$ its complex conjugate.

For SNP measurements the components of the polarization vectors $\mathbf{P}_i$ and $\mathbf{P}_f$ are defined such that $\mathbf{x}$ coincides with the scattering vector $\mathbf{Q}$, the axis $\mathbf{z}$ is perpendicular to the scattering plane (up direction) and $\mathbf{y}$ is chosen to form a right-handed coordinate system. Table XI shows the results of the measurement on the magnetic satellite reflection $(002)^-$ at $T=2$ K. To discuss the SNP results, we note first that the vector $\mathbf{F}_{M\perp}$ is real for TSWs and complex for helical structures. For an incident polarization $\mathbf{P}_i\|\mathbf{Q}(=\mathbf{x})$, the second term in Eq. (8) is zero, as $\mathbf{P}_i$ is perpendicular to $\mathbf{F}_{M\perp}$. The last term, which has a chiral form, is zero when $\mathbf{F}_{M\perp}$ is real (TSW structure) or creates a component along $\mathbf{x}$ for a complex $\mathbf{F}_{M\perp}$ (helix structure). In both cases, the polarization is flipped by π due to the first term of Eq. (8) and the final polarization is expected to be parallel to $-\mathbf{x}$ (compare the first two columns of Table XI). For $\mathbf{P}_i\|\mathbf{y}$ and $\mathbf{z}$, the first two terms of Eq. (8) create components for $\mathbf{P}_f$ which lie in the $(\mathbf{y},\mathbf{z})$ plane (perpendicular to $\mathbf{Q}$). A finite component in the final polarization along $\mathbf{x}$ [$P_{f,x}=(-0.27\pm0.06)$ for $\mathbf{P}_i\|\mathbf{y}$ and $P_{f,x}=(0.28\pm0.06)$ for $\mathbf{P}_i\|\mathbf{z}$] can only occur if the chiral term has a non-zero value. Hence, $\mathbf{F}_{M\perp}$ has to be complex. This confirms that a TSW state can be excluded and consequently the magnetic structure of CuB_2O_4 in the incommensurate phase is a helix.

TABLE XI. Initial $\mathbf{P}_i$ and final $\mathbf{P}_{f,(002)}$ polarizations of the satellite reflection $(002)^-$.

$\mathbf{P}_i$	$\mathbf{P}_{f,(002)^-}$
$\begin{pmatrix}1.00(1)\\0.01(1)\\0.02(2)\end{pmatrix}$	$\begin{pmatrix}-0.87(7)\\-0.03(3)\\-0.07(6)\end{pmatrix}$
$\begin{pmatrix}0.01(1)\\1.00(1)\\0.02(1)\end{pmatrix}$	$\begin{pmatrix}-0.27(6)\\0.47(7)\\-0.21(7)\end{pmatrix}$
$\begin{pmatrix}0.01(1)\\0.01(1)\\0.99(1)\end{pmatrix}$	$\begin{pmatrix}0.28(6)\\0.15(7)\\-0.19(7)\end{pmatrix}$

SNP showed that most of the measured magnetic satellite reflections showed strong depolarization. Depolarization is characteristic of a domain structure, thus we ascribe this depolarization to the existence of more than one magnetic domain of the helical phase.

V. DIFFUSE SCATTERING

For temperatures close to a magnetic phase transition, short-ranged correlated magnetic regions are always found. These give rise to diffuse neutron scattering. For conventional three-dimensional antiferromagnets this critical scattering is usually sizable within a small temperature range only around the Néel temperature T_N. This is in contrast to what is observed in CuB_2O_4, as we shall show below.

The $(\mathbf{q},\omega)$-dependent scattering function $S(\mathbf{q},\omega)$ is related to the imaginary part of the wave-vector dependent static susceptibility $\chi''_{\mathbf{q}}$ through the Kramers-Kronig relation

$$\chi''_{\mathbf{q}}(T)=\mu_B^2\int_{-\infty}^{\infty}[1-\exp(-\hbar\omega/k_BT)]\frac{S(\mathbf{q},\omega)}{\omega}d\omega. \tag{10}$$

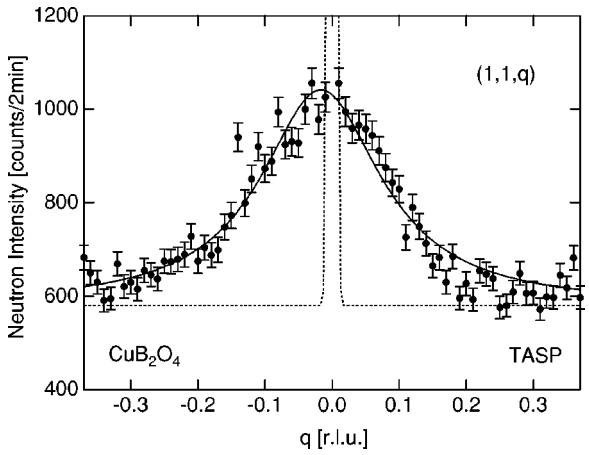

FIG. 7. Typical q scan taken at $T=21.5$ K in CuB_2O_4 on the triple-axis spectrometer TASP operated at a fixed incident neutron wave vector $\mathbf{k}_i=1.97$ Å^{-1}. The dotted line corresponds to the magnetic Bragg reflection (1,1,0) plus background, the solid line to the diffuse magnetic intensity approximated by a Lorentzian function.

Figure 7 shows a typical q-scan along the tetragonal axis taken at $T=21.5$ K from CuB_2O_4 on the triple-axis spectrometer TASP (SINQ) operated with a fixed incident neutron wave-vector $\mathbf{k}_i=1.97$ Å^{-1}. For these measurements, the analyzer was removed from the beam, so that the integration over energy is automatically performed up to energies $\hbar\omega=8$ meV and the neutron spectra directly reflect $\chi_{\mathbf{q}}(T)$. The q-dependent susceptibility for three-dimensional isotropic Heisenberg systems and $T\neq T_N$, is correctly approximated by a Lorentzian function $\chi_{\mathbf{q}}(T)=A/(\kappa^2+q^2)$, where κ is the inverse correlation length.[14] We find that κ follows a power law of the form $(T-T_N)^{-\nu}$ in the paramagnetic phase, with $\nu=0.41\pm0.04$, which is slightly below the mean-field value $\nu=0.5$. Surprisingly, the value of κ does not go to zero at the Néel temperature T_N (see Fig. 8). Upon lowering the temperature below T_N diffuse scattering is observed in the complete commensurate phase when q scans are performed along the [0,0,q] direction. This indicates that small-sized magnetic domains persist along the tetragonal axis well below the Néel temperature. At $T\sim19$ K the correlation length is $\xi=140$ Å and slowly decreases to $\xi=100$ Å at $T=11$ K. Upon approaching the incommensurate-commensurate phase transition the correlation length increases rapidly and diverges at $T^*\sim9.5\pm0.1$ K following the powerlaw $\xi\propto|T-T^*|^{0.40\pm0.05}$. Immediately below T^*, it is difficult to obtain reliable fits from the critical scattering data as the diffuse scattering splits into two symmetric parts on either side of the commensurate Bragg peaks. However, diffuse scattering is still present at the feet of the magnetic satellites and can be observed down to $T=1.5$ K.[2] No diffuse scattering was observed around the magnetic reflections (0,0,2), neither in the commensurate, nor in the incommensurate magnetic phase. As neutron scattering probes only magnetic fluctuations which are perpendicular to the scattering vector **Q**, this shows that the magnetic fluctuations are connected to spin fluctuations perpendicular to the tetragonal axis. Also, because the mean square local amplitude of the spin density $\mathbf{S}_L^2$ is given by $\mathbf{S}_L^2\sim\Sigma_q(\langle\mathbf{S}_q\rangle^2+\langle|\delta\mathbf{S}_q|^2\rangle)$, where the mean-square amplitude of the q component is $\langle|\delta\mathbf{S}_q|^2\rangle=1/2\pi\int d\omega S(q,\omega)$, it is tempting to relate the diffuse scattering observed in CuB_2O_4 with spin fluctuations of Cu(B) spins. In that case, we can conclude that diffuse scattering below T_N describes transverse fluctuations that arise when the B spins tend to be aligned in the basal plane.

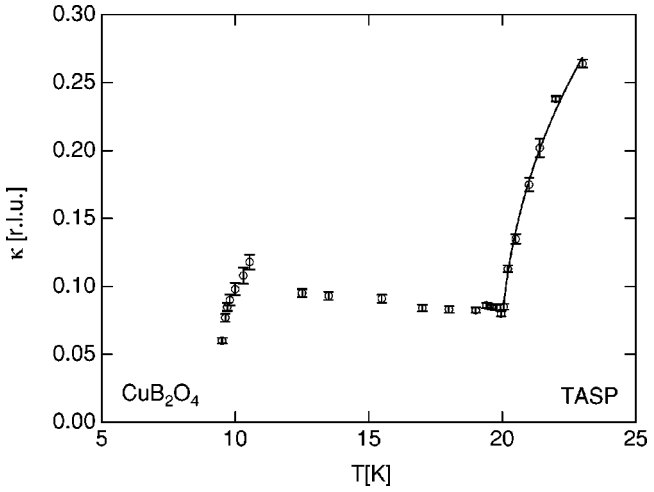

FIG. 8. Temperature dependence of the inverse of the correlation length. The solid line is a fit to the data as explained in the text.

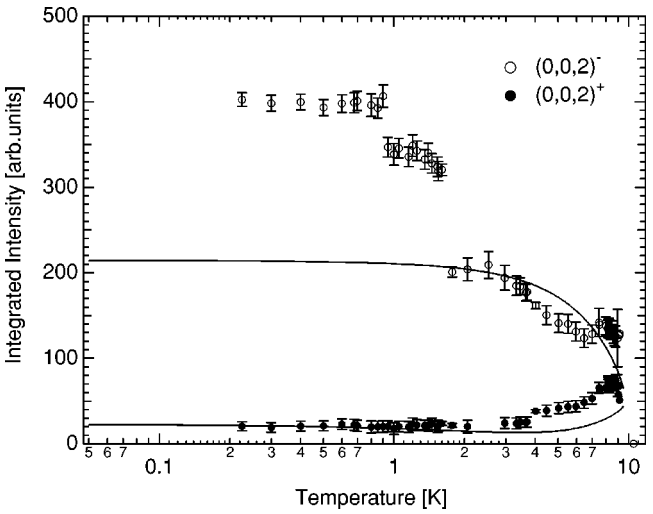

FIG. 9. Intensity of the (002) satellite peaks integrated along the $[0,0,q]$ direction as a function of temperature. The lines correspond to the assumptions $\varphi\propto(T-T^*)$ with $T^*=10$ K and $\mu_{Cu(B)}\propto\sqrt{T^*-T}$. See the text for details.

VI. DISCUSSION AND CONCLUSION

Figure 9 shows the temperature dependence of the magnetic satellites around the (002) nuclear Bragg reflection. Like the other measured magnetic reflections, we find that the satellites with indices $(002)^+$ and $(002)^-$ have unequal intensities. We note first that because neutrons are scattered by the spin components which are perpendicular to the scattering vector, the parameter c_3 (see above) does not influence

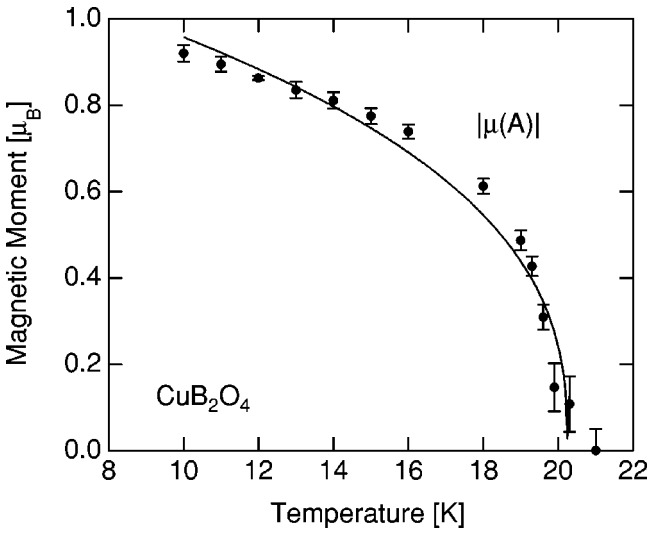

FIG. 10. Temperature dependencies of the size of the magnetic moment $|\mu(A)|$. See the text for details.

the magnetic intensities with indices $(001)^{\pm}$ and second that the magnitude of the Cu(A) moments remains constant when passing into the incommensurate phase. In order to reproduce the temperature dependence of the satellite intensities shown in Fig. 9, we assumed that the magnetic moment in the B sublattice, $\mu_{Cu(B)}(T)$, follows the mean-field power law $\mu_{Cu(B)}(T) \propto \sqrt{T^* - T}$. The results of the calculations are shown as solid lines in Fig. 9. The agreement with the measurement is reasonable down to $T \sim 1.8$ K if we take $\varphi(T) \propto (T - T^*)$. The discontinuity in the temperature dependence of the magnetic intensity at $T = 1.8$ and 1 K seem hence to be related either to a discontinuous change in φ or to a sudden increase of the magnetic moments in the Cu(B) sublattice.

Because the Cu(B) moments are aligned along the tetragonal axis in the commensurate phase, the staggered magnetization of the Cu(A) sublattice can be extracted in the commensurate phase directly from the temperature dependence of the (002) Bragg reflection. As shown in Fig. 10, the size of the Cu (A) moments increases rapidly below T_N and approaches the saturation value of a free $S = 1/2$ Cu^{2+} ion near the commensurate-incommensurate critical temperature T^*. For comparison, the solid line follows the power law $|T - T_N|^{-\beta}$, with the critical exponent $\beta = 0.37$ for a three-dimensional Heisenberg model.[14] The magnetic structure in the commensurate phase is dominated by the Cu(A) moments which form the antiferromagnetic ''cage'' (see Fig. 4), whereas the Cu(B) spins remain essentially disordered. This indicates that exchange interactions within the two copper sub-systems are completely different. In fact the analysis of inelastic neutron diffraction experiments in copper metaborate has shown that the magnetic excitation spectra, taken at $T = 12$ K, are well explained by two independent magnetic sublattices.[12] A strong isotropic antiferromagnetic exchange interaction between nearest Cu(A) moments stabilizes the magnetic ordering of the cage down to T^*. On the other hand it appears that the exchange interactions within Cu(B) spins are frustrated which prevents a magnetic ordering above T^*. Below that temperature, the size of the Cu(B) moments grows and the mutual interactions between the two sublattices become important. Because the Dzyaloshinskii-Moriya interaction is allowed by symmetry on both sites, the two sublattices enter together into an helical state at T^* with a temperature dependent periodicity which decreases as long as the size of the Cu(B) moments grows. Though, the value of $|\mu(B)| \sim 0.5\mu_B$ at temperature $T < 2$ K is still reduced probably as a consequence of frustration. A deeper understanding of the magnetic properties of copper metaborate through the incommensurate-commensurate phase and in the incommensurate phase requires an analysis of the magnetic excitation spectrum at these temperatures.

ACKNOWLEDGMENTS

It is our pleasure to thank A. Furrer, M. Sigrist, and M. Popov for helpful discussions. This work was partially performed at the spallation neutron source SINQ, Paul Scherrer Institut, Villigen, Switzerland. We are also very grateful for the support and allocated beam time at the Institut Laue Langevin, Grenoble, France.

*Electronic address: boehm@ill.fr

[1] G. Petrakovskii, D. Velikanov, A. Vorontinov, A. Balaev, K. Sablina, A. Amato, B. Roessli, J. Schefer, and U. Staub, J. Magn. Magn. Mater. **205**, 105 (1999).

[2] B. Roessli, J. Schefer, G. Petrakovskii, B. Ouladdiaf, M. Boehm, U. Staub, A. Vorontinov, and L. Bezmartenikh, Phys. Rev. Lett. **86**, 1885 (2001); G.A. Petrakovskii, M.A. Popov, B. Roessli, and B. Ouladdiaf, JETP **93**, 809 (2001).

[3] M. Boehm, B. Roessli, J. Schefer, B. Ouladdiaf, A. Amato, C. Baines, U. Staub, and G.A. Petrakovskii, Physica B **318**, 277-281 (2002).

[4] F. Tasset, P.J. Brown, E. Lelièvre-Berna, T. Roberts, S. Pujol, J. Allibon, and E. Bourgeat-Lami, Physica B **267-268**, 69 (1999).

[5] M. Blume, Phys. Rev. **130**, 1670 (1963).

[6] J. Rodriguez-Carvajal, ''FULLPROF: A Program for Rietveld Refinement and Pattern Matching Analysis''; Abstracts of the Satellite Meeting on Powder Diffraction of the XV Congress of the IUCr, p. 127, Toulouse, France (1990).

[7] P.J. Brown, J. Neutron Res. **4**, 2 (1996).

[8] A.S. Wills, Physica B **276-278**, 680 (2000); SARA*h*, Simulated Annealing and Representational Analysis. Programs available from ftp.ill.fr/pub/dif/sarah/.

[9] E. Lelièvre-Berna, Proc. SPIE **4785**, 112 (2002).

[10] M. Martinez-Ripoll, S. Martinez-Carrera, and S. Garcia-Blanco, Acta Crystallogr., Sect. B: Struct. Crystallogr. Cryst. Chem. **27**, 677 (1971).

[11] See, e.g., E. F. Bertaut, in *Magnetism*, edited by T. Rado and H. Suhl (Academic Press, New York, 1963), Vol. III, pp. 149–209.

[12] M. Boehm, S. Martynov, B. Roessli, G. Petrakovskii, and J. Kulda, J. Magn. Magn. Mater. **250C**, 313 (2002).

[13] V. Kovalev, *Irreducible Representations of the Space Groups* (Gordon and Breach, New York, 1965).

[14] M. F. Collins, in *Magnetic Critical Scattering* (Oxford University Press, New York, 1989).